

This item is the archived peer-reviewed author-version of:

Tailoring weak and metallic phases in a strong topological insulator by strain and disorder :
conductance fluctuations signatures

Reference:

Shafiei Mohammad, Fazileh Farhad, Peeters François, Milošević Milorad.- Tailoring weak and metallic phases in a strong topological insulator by strain and disorder : conductance fluctuations signatures
Physical review B / American Physical Society - ISSN 2469-9969 - 109:4(2024), 045129
Full text (Publisher's DOI): <https://doi.org/10.1103/PHYSREVB.109.045129>
To cite this reference: <https://hdl.handle.net/10067/2047650151162165141>

Tailoring weak and metallic phases in a strong topological insulator by strain and disorder: conductance fluctuations signatures

Mohammad Shafiei,^{1,2} Farhad Fazileh,² François M. Peeters,^{3,1} and Milorad V. Milošević^{1,4,*}

¹*Department of Physics, University of Antwerp, Groenenborgerlaan 171, B-2020 Antwerp, Belgium*

²*Department of Physics, Isfahan University of Technology, Isfahan 84156-83111, Iran*

³*Departamento de Física, Universidade Federal do Ceara, 60455-760 Fortaleza, Ceara, Brazil*

⁴*NANOlaboratory Center of Excellence, University of Antwerp, Belgium*

(Dated: April 8, 2024)

Transport measurements are readily used to probe different phases in disordered topological insulators (TIs), where determining topological invariants explicitly is challenging. On that note, universal conductance fluctuations (UCF) theory asserts the conductance G for an ensemble has a Gaussian distribution, and that standard deviation δG depends solely on the symmetries and dimensions of the system. Using a real-space tight-binding Hamiltonian on a system with Anderson disorder, we explore conductance fluctuations in a thin Bi_2Se_3 film and demonstrate the agreement of their behavior with UCF hypotheses. We further show that magnetic field applied out-of-plane breaks the time-reversal symmetry and transforms the system's Wigner-Dyson class from symplectic to unitary, increasing δG by $\sqrt{2}$. Finally, we reveal that while Bi_2Se_3 is a strong TI, weak TI and metallic phases can be stabilized in presence of strain and disorder, and detected by monitoring the conductance fluctuations.

I. INTRODUCTION

Topological insulators (TIs) are characterized by their insulating behavior in the bulk, while maintaining conducting states on their surfaces or edges¹⁻³. The investigation and characterization of topological states in materials, notably the TI phase, have garnered considerable attention in the past few years. This enthusiasm stems from the significant value of these states concerning fundamental concepts as well as potential applications^{4,5}, and has instigated a pertinent search for novel materials that can host topological phases. In topological quantum chemistry for example, one can determine the topological properties of nonmagnetic substances by their symmetries and their orbitals' position and type. Using this method, it was recently found that a significant proportion of the Inorganic Crystal Structure materials exhibit unique topological phases⁶. Specifically, the research revealed that over 27% of these materials possess topological characteristics, while about 12% can be classified as topological insulators⁶.

To date, Bi_2Se_3 family of materials are the best-known three-dimensional TIs. These materials all belong to the symmetry group No.166, which contains the most significant number of TIs (410)^{6,7}. Bi_2Se_3 has been the subject of broad theoretical and experimental research, due to its simple band structure and single Dirac cone at its surfaces. Surface states in Bi_2Se_3 , Bi_2Te_3 , and Sb_2Te_3 are protected by time-reversal symmetry (TRS). These materials also exhibit strong spin-orbit coupling (SOC)^{7,8}. They belong to the symplectic ensemble based on the Wigner-Dyson classification, which introduced the Hamiltonian Gaussian distribution and the categorization of systems based on symmetries⁹. The Wigner-Dyson classification¹⁰ generally classifies systems into the three ensembles listed in Tab. I.

Following the discovery of TIs, most research was fo-

cused on samples with maximal possible purity. That said, the ever-present disorder in all materials and devices of interest, resulting from impurities and/or lattice defects, is unavoidable^{11,12}. Due to strong SOC between multiple orbits, but also decoherence caused by temperature and disordered vacancies, it becomes challenging to interpret experimental data^{13,14}. In a transport measurement, the quantum interference between all possible electron paths between two sites in a sample makes electrical conduction sensitive to the Fermi energy, magnetic field, and impurity configuration^{15,16}. Hence one looks to conductance and its fluctuations to extract any additional information that helps monitor the properties of the TI under investigation. In fact, by analyzing the conductance and its fluctuations, one may determine more about the topological properties of the system. For example, introducing dilute nonmagnetic impurities to a TI cannot affect the topological phase of the material, as demonstrated by measuring surface state transport and observing the absence of departure in conductance from the quantized value. This is however only feasible with parallel advances in theoretical studies of conductance fluctuations in TIs. On that front, the universal conductance fluctuations (UCF) theory was developed to capture mesoscopic quantum interference effects and dis-

TABLE I. Wigner-Dyson classification of materials, into three ensembles based on time-reversal (TRS) and spin-rotation (SRS) symmetry.

	TRS	SRS	Ensemble
$\beta = 1$	✓	✓	<i>orthogonal</i>
$\beta = 2$	✗	✗ or ✓	<i>unitary</i>
$\beta = 4$	✓	✗	<i>symplectic</i>

tinctive characteristics of quantum transport in TIs¹⁷, as discovered by exploring the magnetoresistance of a small-scale conductor^{18–20}.

The resistance of a large-scale conductor is given by $R = \rho L/S$, where ρ denotes resistivity, and L and S represent the length and cross-sectional area, respectively. According to the diffusive transport mechanism, once the size of the system is reduced down to the coherence length L_ϕ (also known as the dephasing length), the above resistance relation breaks down, and in this regime, the ability of a material to conduct electric current is directly expressed in terms of conductance. Electrons' complicated and varied diffusion path through a conductor is known as the Feynman path. By decreasing the size of the Feynman path, quantum correction becomes increasingly relevant. Although the conductance G varies from sample to sample owing to different impurity configurations that cause different Feynman paths, the root mean square conductance δG is the *same* for all samples. δG is suppressed if the system is not coherent, that is, if the sample size is larger than L_ϕ ²¹.

According to the UCF theory, given an ensemble of diffusive metals, the conductance G has a Gaussian distribution with a constant width δG that depends only on the symmetries and dimension of the system. Conductance fluctuations in TI at zero temperature can be predicted using the key parameters in UCF, which include the Wigner-Dyson parameter β , Kramer's degeneracy s , and the number of independent eigenmodes of the Hamiltonian k ^{12,21}. The UCF amplitude is given by:

$$\delta G = c_d \sqrt{\frac{k s^2}{\beta}}, \quad (1)$$

where c_d is a constant that depends on the dimension (d) of the system and is related to the ratio of the sizes L_x , L_y , and L_z of the system. For the three-dimensional system where the length ratio is considered as $L_z/L_{x,y} = 1$, $c_d = 0.55$, and the value of c_d will decrease (increase) slightly as the length ratio increases (decreases), as shown in Ref. 12. According to the Wigner-Dyson classification, the β symmetry parameter takes the values 1, 2, or 4.

This paper analyzes conductance fluctuations (CFs) in Bi_2Se_3 -film using a real-space tight-binding Hamiltonian and considering Anderson disorder, to validate to which extent their behavior aligns with the expectations posed by UCF theory. Within the CF analysis, we further provide evidence that introduction of an out-of-plane magnetic field breaks TRS and causes a transition of the system from symplectic Wigner-Dyson class ($\beta = 4$) to unitary one ($\beta = 2$), accompanied by an increase in δG by a factor of $\sqrt{2}$. Finally, in contrast to the inherent strong topological insulator (TI) properties of Bi_2Se_3 , our study reveals that in presence of strain and disorder this material can exhibit weak TI and metallic phases, as evidenced by the corresponding CF signatures.

This paper is organized as follows. Sec. II contains the theoretical framework, and introduces the structure

of Bi_2Se_3 , the real-space tight-binding Hamiltonian, and inclusion of Anderson disorder. The Landauer-Büttiker approach used for transport calculations is also outlined within this section. Sec. III is devoted to the investigation of conductance fluctuations in a 3D TI. First, $\langle G \rangle$ and δG are calculated for Bi_2Se_3 , showing that the surface states are robust against disorder. The behavior of CFs with change of thickness and Fermi energy of the sample is also investigated. Next the effect of the applied out-of-plane magnetic field is discussed, and the corresponding change of the class of the system. In Sec. IV, the effect of strain is investigated using transport calculations, to reveal transitions between the strong, weak, and metallic phases in disordered TI film of Bi_2Se_3 . Our summary and conclusions are given in Sec. V.

II. THEORETICAL FRAMEWORK

A. Material structure and tight-binding Hamiltonian

As said above, Bi_2Se_3 family of materials are archetypal three-dimensional TIs, having simple surface band structure and a single Dirac cone therein. Another advantage of these TIs is a relative large bulk band gap, roughly 0.3 eV for Bi_2Se_3 , that provides a large window for the topological states. Bi_2Se_3 has a rhombohedral structure in which five Se-Bi-Se-Bi-Se atomic layers are periodically stacked; these layers are known as quintuple layers (QLs), and thickness of each QL is about 1 nm^{22,23}.

Bi_2Se_3 structure possesses threefold rotational symmetry around the z -axis, twofold rotational symmetry around the x -axis, inversion symmetry, and TRS^{22,24}. This material family belongs to the symmetry group $D_{3d}^5(R\bar{3}m)$, in which D_{3d} is the direct multiplication of D_3 and the inversion operator group. To describe the system, we consider an effective real-space tight-binding Hamiltonian in which each unit cell is assumed to contain two atoms (Bi, Se) and spin. Taking into account just the nearest neighbors, each unit cell will have six x - y in-plane neighbors coupled by vectors \mathbf{n}_i ($i=1,2,3$) and two z out-of-plane neighbors connected by vector \mathbf{n}_4 . The real-space Hamiltonian is as follows^{25,26}:

$$H = \sum_i c_i^\dagger E_{on} c_i + \sum_{i,\alpha} (c_i^\dagger T_\alpha c_{i+\alpha} + H.c.), \quad (2)$$

where $\alpha = \mathbf{n}_1, \mathbf{n}_2, \mathbf{n}_3, \mathbf{n}_4$, and the operator c_i^\dagger (c_i) creates

TABLE II. Hopping parameters for the real-space tight-binding Hamiltonian for Bi_2Se_3 .

A_\parallel (eV)	A_z (eV)	E_0 (eV)	B_\parallel (eV)
0.5	0.44	0.29	0.25
B_z (eV)	C_0 (eV Å)	C_\parallel (eV Å ²)	C_z (eV Å ²)
0.25	-0.0063	6.65	-1.75

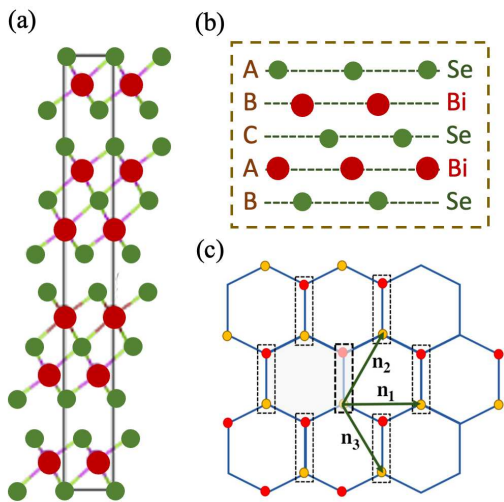


FIG. 1. (a) Bi_2Se_3 crystal structure. (b) A quintuple layer (QL) of Bi_2Se_3 . The atoms are stacked in layers in the z direction in an ABCABC sequence. (c) Lattice structure of Bi_2Se_3 in the x - y plane. Each unit cell has two neighboring unit cells in the z direction connected by vector \mathbf{n}_4 , and six neighboring unit cells in the x - y plane connected by vectors $\mathbf{n}_{1,2,3}$.

(annihilates) an electron at site i . Further we have:

$$E_{on} = (E_0 - 2\Sigma_\alpha B_\alpha)\sigma_z \otimes \sigma_0, \quad (3)$$

and

$$T_\alpha = C_\alpha \sigma_0 \otimes \sigma_0 + B_\alpha \sigma_z \otimes \sigma_0 - i\left(\frac{A_\alpha}{2}\right)\sigma_x \otimes \sigma \cdot \mathbf{n}_\alpha. \quad (4)$$

The onsite energy (E_{on}) and the hopping parameters (T_α) between unit cells are represented by 4×4 matrices and their parameters are listed in Tab. II. Without losing generality, we assume particle-hole symmetry and $C_\alpha=0$. \mathbf{n}_i vectors are defined based on the structure of the system as $\mathbf{n}_1 = (1/2, \sqrt{3}/2, 0)$, $\mathbf{n}_2 = (-1/2, \sqrt{3}/2, 0)$, $\mathbf{n}_3 = (1, 0, 0)$, $\mathbf{n}_4 = (0, 0, 1)$.

B. Anderson disorder

Disorder in a lattice may take the form of undesirable dislocations, vacancies, or inclusions, and here we model it as Anderson disorder. In what follows, W_i indicates the strength of disorder at each site of the lattice, of randomly distributed strength in the interval $[-W/2, W/2]$, added to the system with the following Hamiltonian^{12,27}:

$$H_D = \sum_{i,\alpha} W_i c_{i,\alpha}^\dagger c_{i,\alpha}. \quad (5)$$

As previously stated, the disorder in a structure is often induced by unwanted defects. However, deliberate surface disorder may also be used for device engineering. In 3D TIs, surface disorder, for instance, may be utilized

to regulate the transport of surface states. For example, in Ref. 28, a practicable strategy for systematically controlling transport on the surface of a three-dimensional TI was realized by introducing intense disorder (close to the threshold strength to convert TI to a trivial phase) within a controlled depth from the surface of the TI. This procedure can then be applied to manufacture integrated TI circuits.

C. Transport formalism

The standard method for determining the phase transition in disordered systems is a finite-size scaling analysis of the localization length. In some cases the localization length diverges, so its use to examine the disordered phase diagram becomes challenging. Instead, alternative approaches, such as the investigation of conductance, are employed²⁹.

The Landauer-Büttiker formalism uses the scattering amplitude of electrons to obtain the conductivity properties in a quantum junction and is used for transport calculations in non-interacting nanostructure systems, in the absence of a phase-breaking environment in which quantum coherence is maintained. The conductance at zero temperature was investigated using Landauer's scattering method, which yielded the following relationship:

$$G = \frac{e^2}{h} \sum_n T_n(E_F), \quad (6)$$

where T_n is the probability of transmission in the n -th channel. Since atomic-scale systems are typically described by discrete models, transport is calculated via the Green's function formulation. The effect of electrodes is implemented as self-energy. Under time-symmetry, Green's function is divided into two retarded (advanced) portions with propagation into the future (past) and are defined as follows³⁰:

$$\begin{aligned} \hat{G}^R(E) &= [(E + i\eta)\hat{I} - \hat{H}]^{-1}, \\ \hat{G}^A(E) &= [\hat{G}^R(E)]^\dagger. \end{aligned} \quad (7)$$

The Hamiltonian of the whole system is as follows:

$$\begin{bmatrix} H_L & V_{LC} & 0 \\ V_{CL} & H_C & V_{CR} \\ 0 & V_{RC} & H_R \end{bmatrix}, \quad (8)$$

where the sample Hamiltonian is indicated by H_C , whereas the Hamiltonian matrices of the left electrode and right electrode are denoted by H_L and H_R , respectively. The non-diagonal elements represent the sample's coupling with the electrodes, and since H must be Hermitian, $V_{CL}=V_{LC}^\dagger$ and $V_{CR}=V_{RC}^\dagger$. The effect of leads is described by the self-energy Σ :

$$G_C^R(E) = [E - H_C - \Sigma^R]^{-1}, \quad (9)$$

and the transmission function is expressed as follows:

$$T(E) = \text{Tr}[\Gamma_L(E)G^R(E)\Gamma_R(E)G^A(E)], \quad (10)$$

where $\Gamma = i(\Sigma^R - \Sigma^A)$.

Considering that we are dealing with a multi-component system (including the electrodes), the recursive Green's function method is applied, since the Green's functions of isolated subsystems (with Hamiltonians H_c , H_L , H_R) and the coupling matrices between subsystems (V_{CL} , V_{LC} , V_{CR} , V_{RC}) are known. It is an advantageous method to calculate the relevant Green's function components for large complex systems which can be divided into many connected parts. Starting at one end of the system, the subsystems are added one by one, finally the full Green's function of the whole system can be found. Taking into account the Green's function for each subsystem (G_0) and the coupling matrix between them (V), the full Green's function (G) can be expressed as $G = G_0 + G_0VG$ through the Dyson equation. From a computational perspective, the use of recursive methods may provide much quicker results compared to directly solving equations, particularly for large-scale systems³¹.

III. FUNDAMENTALS OF CONDUCTANCE FLUCTUATIONS IN Bi_2Se_3 FILM

In this section we will examine numerically the fluctuations of conductance in disordered Bi_2Se_3 , to compare their behavior to the UCF theory. UCF asserts that for an ensemble of diffusive metals, the conductance has a Gaussian distribution with a constant standard deviation δG , which depends on the symmetries and dimensions of the system, as discussed regarding Eq. (1). The conductance fluctuation $\delta G = \langle (G - \langle G \rangle)^2 \rangle^{1/2}$ is defined as the standard deviation of conductance for a disordered ensemble and is averaged over all ensembles.

Fig. 2 illustrates the average conductance $\langle G \rangle$ and conductance fluctuation δG for various disorder values and $E_F = 0.05$ and 0.2 eV for a sample with a thickness of 4 quintuple layer (QL), and in-plane lattice site $L_x = L_y = 10$. Three-dimensional TI consists of bulk insulating states and conducting spin-momentum-locked dissipationless surface states. ARPES experimentally validated these surface states' features, including a Dirac cone protected by TRS. In Fig. 2, the Fermi energy of 0.05 eV is related to surface states, and for a weak disorder, conductance fluctuations are negligible, illustrating the robustness of surface states against disorder. The conductance fluctuations approach the value $\delta G \approx 0.28$ as the disorder in the system increases, which agrees with UCF theory, given that the system belongs to the symplectic class ($c_d \approx 0.55$, $\beta = 4$, $s = k = 1$ in Eq. (1)). Increasing the disorder beyond sufficient magnitude ($W > 7$ eV) causes δG to decrease toward zero, illustrating that the system enters the metallic phase as shown in Fig. 2(b).

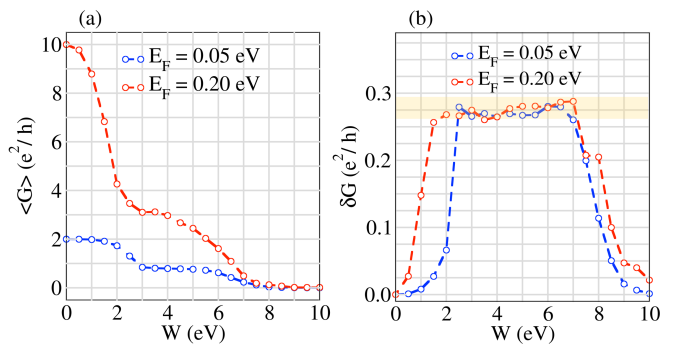


FIG. 2. (a) The mean conductance $\langle G \rangle$ and (b) the standard deviation of conductance δG of disordered Bi_2Se_3 as a function of disorder strength W , with $N_{QL} = 4$ and the number of in-plane sites $L_x = L_y = 10$. $E_F = 0.05$ eV is related to surface states (any $E_F < 0.15$ eV is), and as shown in panel (b), conductance fluctuations are negligible for weak disorder, indicating surface states' robustness to disorder.

The spatial dimension of the sample is one of the deterministic factors of the conductance fluctuation amplitude. As mentioned previously, the coefficient c_d in Eq. (1) actually depends on N_{QL}/L_x and N_{QL}/L_y length ratios, as calculated in Ref. 12, and verified here (as shown in Fig. 3(b)). For three-dimensional sample the length ratios are considered as $N_{QL}/L_{x,y} = 1$, in which case $c_d = 0.55$, and change in length ratios will cause a some deviation in c_d . Fig. 3(a) shows our data, plotting the dependence of δG on N_{QL} for $W = 3, 4$ eV while L_x and L_y are fixed. Since $N_{QL} < L_x, L_y$ in the thin film, δG is nearly constant in this regime, but its decrease as a

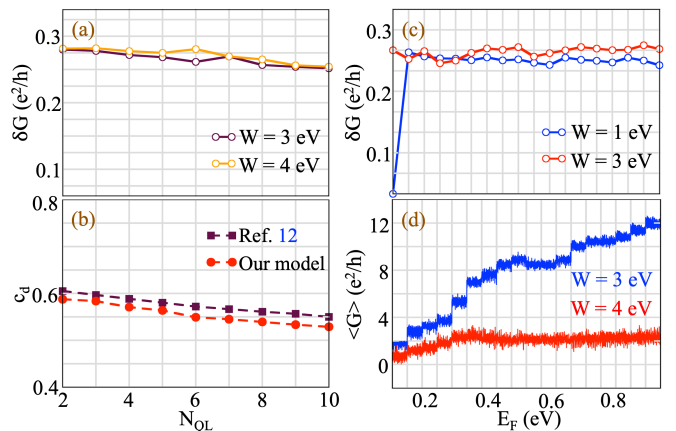


FIG. 3. (a) Conductance fluctuation versus the thickness of the sample N_{QL} . δG depends on N_{QL}/L_x and N_{QL}/L_y ratio, and the conductance fluctuations are almost constant, for fixed L_x and L_y of the thin film. (b) c_d values calculated here, compared to those extracted from Ref. 12, as a function of thickness. (c) Conductance fluctuation versus Fermi energy. Considering the symplectic class where SR symmetry does not exist, increasing the Fermi energy does not change the Wigner-Dyson class of the sample. (d) Conductance versus Fermi energy for 200 samples for each E_F .

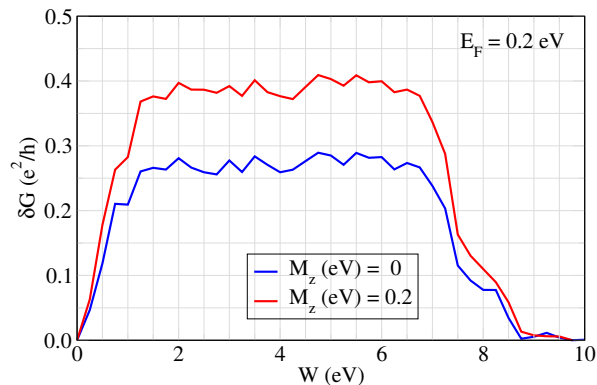


FIG. 4. Magnetization of the system leads to TRS collapse, a change from symplectic ($\beta=4$) to unitary ($\beta=2$) class, and a $\sqrt{2}$ -fold rise in δG in the absence of TRS.

function of N_{QL} does follow the expected decrease in c_d due to the increasing $N_{QL}/L_{x,y}$ ratio.

Bi_2Se_3 belongs to the symplectic class ($\beta=4$) in the Wigner-Dyson classification, where TRS is preserved, but SR symmetry is not. So long as disorder is weak or the localization length is much larger than the spin relaxation length, the SOC is considerable, and the system lacks SR symmetry. In systems where the localization length is less than the spin relaxation length and the kinetic energy is larger than the SOC term, SOC may be ignored. In these systems SR symmetry is established such that the system belongs to the orthogonal class ($\beta=1$). Fig. 3(c) shows the conductance fluctuation as a function of Fermi energy for $W = 1$ eV and 3 eV. For weak disorder (such as $W = 1$ eV) and small Fermi energies (inside the bulk gap) that include only the surface states bands, $\delta G=0$ indicates the robustness of surface states in 3D TI against disorder. Since the surface states in a strong TI are robust to impurities that preserve TRS, there will not be any deviation in conductance for weak disorder and the conductance will remain quantized. Consequently, the conductance of surface states (G) does not deviate from the quantized value for weak disorders in different ensembles, yielding $\delta G=0$. Since Bi_2Se_3 is in the symplectic class, in which SR symmetry does not exist, the system's Wigner-Dyson class remains unchanged. Fig. 3(d) also depicts the variations in conductance versus Fermi energy for 200 samples for each E_F .

To further validate UCF numerically, we examine the effect of magnetic field \mathbf{B} on 3D disordered TI, leading to TRS breakdown and changing the class of the system. The external magnetic field \mathbf{B} is composed of two parts, and the first is the Zeeman term, represented by:

$$H_{Zeeman} = M_z \sigma_z \tau_0 + M_x \sigma_x \tau_x + M_y \sigma_y \tau_x, \quad (11)$$

where $M_i (i = x, y, z)$ is the strength of magnetization in i -direction. Modifying the hopping phase by changing the hopping integrals is the second part. For the external magnetic field along the z -axis, $T_x \rightarrow T_x \exp(-i2\pi\Phi)$, where $\Phi = \int \mathbf{A} \cdot d\mathbf{l} / \Phi_0$ and $\Phi_0 = h/e$ represent the mag-

netic quantum flux, while $\mathbf{A} = (-B_z \hat{x}, 0, 0)$ represents the vector potential. Here, we consider only the Zeeman term and magnetization in z -direction, which breaks the TRS and changes the system class from symplectic to unitary. Fig. 4 displays conductance fluctuations (δG) for two situations with and without magnetization. Magnetization causes TRS to collapse, and the system enters the unitary class, where δG changes by a factor of $\sqrt{2}$ when compared to the case when TRS is present, because the conductance standard deviation is proportional to $1/\sqrt{\beta}$ (based on Eq. (1), where β changes from 4 to 2). By applying magnetization to TIs, the surface states of TI are gapped, instead of having the form of a Dirac cone without a gap when TRS is preserved. Depending on the size and direction of the applied magnetization, it can lead to the appearance of topological phases like quantum anomalous Hall, axion insulator, or high-Chern number quantum anomalous Hall phase³².

IV. TUNING THE TOPOLOGICAL PHASES: STRONG, WEAK AND METALLIC PHASES IN TOPOLOGICAL INSULATOR

Topology is the study of characteristics of materials which do not change continuously and the invariant that fits this description is referred to as a topological invariant. In three dimension, TIs are characterized by four indices ($\nu_0; \nu_x, \nu_y, \nu_z$) that may take zero or one and is an ordinary insulator if $(0; 000)$ ³³. The number of Dirac cones on the surface could be viewed as a metric of the bulk topology, so classifying 3D TIs into two categories: strong TI (STI) and weak TI (WTI). If the number of Dirac cones is odd, we will have an STI with $\nu_0 = 1$; if the number of Dirac cones is even, we have a WTI with $\nu_0 = 0$; ν_0 is referred to as a strong index. ν_x, ν_y, ν_z are weak indices, and in the WTI phase, surface states are not formed on the surfaces perpendicular to (ν_x, ν_y, ν_z) ^{1,29}.

Identifying WTI states in three dimensions is challenging since topological surface states exist on only some surfaces. Bi_2Se_3 , Bi_2Te_3 , and Sb_2Te_3 are STI, whereas Sb_2Te_3 is referred to as WTI⁷. In contrast to STI, surface states in WTI are not protected against localization. Applying disorder to WTI may result in losing Dirac state properties and some topological features³⁴.

In this section, we study the topological phase transition from the strong phase to the weak phase for Bi_2Se_3 driven by strain-induced band engineering. Strain is defined as a change in the displacement vector \vec{U} relative to its initial position and in the linear regime may be represented by the following tensor³⁵:

$$\varepsilon_{ij} = \frac{1}{2} \left(\frac{\partial U_i}{\partial x_j} + \frac{\partial U_j}{\partial x_i} \right). \quad (12)$$

The electrical properties of the system and topological nature are affected by a slight strain since the gap of the Bi_2Se_3 family are in the range of 220-300 meV. The strain alters the bond length and angle, hence changing the

Hamiltonian parameters; the values for these parameters are taken from Ref. 36.

The effect of the out-of-plane uniaxial strain is addressed by extending or compressing the z -direction lattice parameter (c) as $\epsilon_{\perp} = \frac{c-c_0}{c_0}$, where c_0 is the z -direction lattice parameter in the strain-free structure. The in-plane biaxial strain is defined as $\epsilon_{\parallel} = \frac{a-a_0}{a_0}$, by stretching or squeezing the lattice parameter in the x - y plane, where a_0 is the unstrained lattice parameter in the x - y plane. The biaxial strain has an indirect influence on the bandgap (Δ_{Γ}), with the parameter c tending to rise for $\epsilon_{\parallel} < 0$ and decrease for $\epsilon_{\parallel} > 0$ ^{35,37}. In our model, we considered the Poisson ratio $\nu = 0.27$ for Bi_2Se_3 , that describes direct dependency of uniaxial out-of-plane strain on the biaxial in-plane strain³⁸, and has been included in all our calculations with strain. The variation of the band gap at the Γ point as a function of out-of-plane and in-plane strain is shown in Fig. 5(a).

Bloch wave functions define topological invariants such as the Chern number and Z_2 in the bulk of materials under translational symmetry. When the translational symmetry is broken, the band structure cannot be used to determine the topological character of the system. The index theorem³⁹, scattering matrix⁴⁰, or transport calculations are often employed in disordered systems to determine the topological phase.

Robustness to disorder is a defining characteristic of TIs, and based on this property, it is possible to distinguish between strong and weak phases in 3D TIs. The absence of backscattering prevents the localization of electrons in surface states, which contributes to the disorder-resistance of Dirac electrons. In the weak TI phase, valleys induced by an even number of Dirac cones

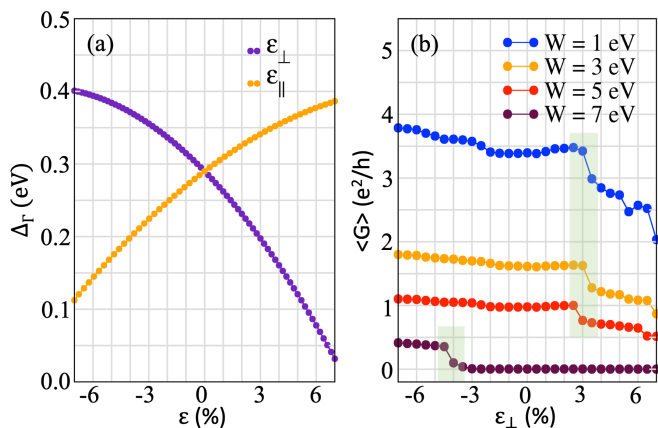


FIG. 5. (a) Bi_2Se_3 bulk gap (Δ_{Γ}) as a function of out-of-plane (ϵ_{\perp}) and in-plane strain (ϵ_{\parallel}). (b) The behavior of conductance in terms of out-of-plane strain for $W=1, 3, 5,$ and 7 eV. In each case, the considered Fermi energy is located on the first conduction band. Transport calculations may be used to identify the topological phase transition in non-translationally symmetric systems. When the system is in a strong phase, changes of $\langle G \rangle$ are minimal and, fluctuations in conductance may be noticed during the weak phase.

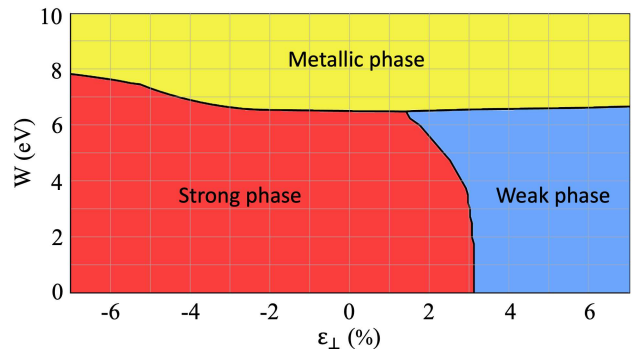


FIG. 6. Phase diagram for strong, weak and metallic states in 3D TI in terms of out-of-plane strain and strength of disorder. Both strong and weak phases exist for weak disorders, and the metallic phase is detectable after sufficiently strong disorder is present.

localize Dirac electrons by intervalley scattering. Translational invariance is lost when disorder is introduced into a system, and standard approaches cannot be used to determine topological invariants. Instead, topological phase transitions may be identified using transport calculations.

Fig. 5(b) depicts the behavior of conductance under out-of-plane strain for $W=1, 3, 5,$ and 7 eV. In each case, we considered Fermi energy crossing the first conduction band. Disorder does not leads to significant conductance fluctuations while the TI is in a strong phase. Still, given significant out-of-plane tensile strain, the system enters the weak phase, where Dirac electrons are localized, and conductance fluctuations are significant.

As shown in Fig. 6, STI and WTI are maintained in the absence of disorder or for disorder values below ~ 7 eV. However, the system transits into the metallic phase for sufficiently large disorder values. When the system is in a strong phase, changes of $\langle G \rangle$ are minimal and, deviations in conductance may be noticed in the weak phase. In the strong disorder region, the bulk band gap is filled by impurity states that overlap to develop extended states, giving rise to the metal phase. This phase diagram is derived from calculations of $\langle G \rangle$ as a function of W and ϵ_{\perp} (as shown in Fig. 5, for different applied strain and disorder). Specifically, we calculated $\langle G \rangle$ for magnitude of the disorder (W) varied with step size 0.1 eV, the applied strain (ϵ_{\perp}) changed with step size 0.5% , and for different Fermi energies for surface states and bulk regime to create this phase diagram. The drastic change in $\langle G \rangle$ - highlighted in Fig. 5(b) - marks the transition of the TI from strong to weak phase, and $\langle G \rangle = 0$ marks the transition to metallic phase.

Although Bi_2Se_3 is an STI, it has been shown that all three phases, strong, weak, and metallic, may be obtained by altering the system's properties via strain and disorder. The occurrence of strong, weak, and metallic states in a TI is directly related to the characteristics of the band structure of the material, namely the bulk gap

and hopping parameters. The application of strain thus provides an effective method for manipulating the band structure and thereby the fundamental phases of the system. In other words, in a disordered TI, the critical threshold for the phase transition between strong, weak, and metallic states is controllable via band engineering, accomplished by applying appropriate strain. Applying significant compressive strain in the out-of-plane direction directly affects the overlap between bulk and extended states. This overlap is determined by the size of the bulk gap and the in-plane onsite energy hopping B (in Eq.(3)) in the Hamiltonian. Hence, the threshold value for disorder required to transition from a strong phase to a metallic phase increases once disordered TI is subjected to considerable compressive out-of-plane strain.

V. SUMMARY AND CONCLUSIONS

In systems wherein translational symmetry is violated, for instance as a result of disorder, it is challenging to identify the phases of matter by directly calculating topological invariants such as Z_2 . In these cases, transport measurements are a convenient practical tool to examine the system's characteristics and determine its (topological) phases. The universal conductance fluctuation (UCF) theory, according to which the conductance G for an ensemble has a Gaussian distribution and the standard deviation δG depends only on the symmetries and dimensions of the system, is one of the most interesting quantum transport theories for topological insulators. Symmetries in the system are one of the crucial factors for estimating δG using UCF; based on the symmetries, the systems are divided into three ensembles: orthogonal, unitary, and symplectic. This classification is known as the Wigner-Dyson classification, and the sample class

is determined by time-reversal symmetry and spin rotation (SR) symmetry. In this paper, considering a real-space tight-binding Hamiltonian for Bi_2Se_3 , we have explored the conductance fluctuations in disordered Bi_2Se_3 , by performing Landauer-Büttiker transport calculations with random Anderson disorder. The calculated standard deviation of conductance (δG) proved that surface states are robust against disorder. With increasing the strength of disorder, δG approaches 0.28, which is consistent with UCF. By evaluating δG for different Fermi energies, we showed that because Bi_2Se_3 belongs to the symplectic class and lacks SR symmetry, raising the Fermi energy does not change the system's class. On the other hand, with the collapse of TRS by applying an out-of-plane magnetic field, the system does change the class, from symplectic to unitary, as validated by the observed increase in δG with a $\sqrt{2}$ factor. Due to the loss of translational symmetry in the presence of disorder, we further explored the system's topological phases in the presence of strain. We demonstrated that it is indeed feasible for Bi_2Se_3 to exhibit strong TI, weak TI, and metallic phases, as applying strain in the presence of disorder tunes the band structure of the material. In addition to verifying the control of different topological phases by applying strain, the method outlined in this paper provides a direct way to detect these phases in various materials using transport measurements, rather than having to rely on the theoretically calculated topological invariant that is challenging to determine in disordered TIs.

ACKNOWLEDGMENTS

This research was supported by the Research Foundation-Flanders (FWO-Vlaanderen), the Special Research Funds (BOF) of the University of Antwerp, and the Isfahan University of Technology.

* milorad.milosevic@uantwerpen.be

¹ L. Fu, C. L. Kane, and E. J. Mele, *Physical Review Letters* **98**, 106803 (2007).
² M. Z. Hasan and C. L. Kane, *Reviews of Modern Physics* **82**, 3045 (2010).
³ X.-L. Qi and S.-C. Zhang, *Reviews of Modern Physics* **83**, 1057 (2011).
⁴ F. Ortman, S. Roche, and S. O. Valenzuela, *Topological insulators: Fundamentals and perspectives* (John Wiley & Sons, 2015).
⁵ W. Tian, W. Yu, J. Shi, and Y. Wang, *Materials* **10**, 814 (2017).
⁶ M. Vergniory, L. Elcoro, C. Felser, N. Regnault, B. A. Bernevig, and Z. Wang, *Nature* **566**, 480 (2019).
⁷ H. Zhang, C.-X. Liu, X.-L. Qi, X. Dai, Z. Fang, and S.-C. Zhang, *Nature Physics* **5**, 438 (2009).
⁸ Y. Chen, J. G. Analytis, J.-H. Chu, Z. Liu, S.-K. Mo, X.-L. Qi, H. Zhang, D. Lu, X. Dai, Z. Fang, *et al.*, *Science* **325**, 178 (2009).

⁹ P. Adroguer, D. Carpentier, J. Cayssol, and E. Orignac, *New Journal of Physics* **14**, 103027 (2012).
¹⁰ F. J. Dyson, *Journal of Mathematical Physics* **3**, 140 (1962).
¹¹ H.-C. Hsu, I. Klefogiannis, G.-Y. Guo, and V. A. Gopar, *Journal of the Physical Society of Japan* **87**, 034701 (2018).
¹² Y. Hu, H. Liu, H. Jiang, and X. Xie, *Physical Review B* **96**, 134201 (2017).
¹³ Z. Li, Y. Meng, J. Pan, T. Chen, X. Hong, S. Li, X. Wang, F. Song, and B. Wang, *Applied Physics Express* **7**, 065202 (2014).
¹⁴ Z. Li, T. Chen, H. Pan, F. Song, B. Wang, J. Han, Y. Qin, X. Wang, R. Zhang, J. Wan, *et al.*, *Scientific Reports* **2**, 595 (2012).
¹⁵ T. Dietl, *Physical Review Letters* **130**, 086202 (2023).
¹⁶ R. Islam, S. Mardanya, A. Lau, G. Cuono, T.-R. Chang, B. Singh, C. M. Canali, T. Dietl, and C. Autieri, *Physical Review B* **107**, 125102 (2023).

- ¹⁷ E. Akkermans and G. Montambaux, *Mesoscopic physics of electrons and photons* (Cambridge University Press, 2007).
- ¹⁸ C. Umbach, S. Washburn, R. Laibowitz, and R. A. Webb, *Physical Review B* **30**, 4048 (1984).
- ¹⁹ S. Islam, S. Bhattacharyya, H. Nhalil, S. Elizabeth, and A. Ghosh, *Physical Review B* **97**, 241412 (2018).
- ²⁰ D.-H. Choe and K.-J. Chang, *Scientific Reports* **5**, 10997 (2015).
- ²¹ P. A. Lee and A. D. Stone, *Physical Review Letters* **55**, 1622 (1985).
- ²² C.-X. Liu, X.-L. Qi, H. Zhang, X. Dai, Z. Fang, and S.-C. Zhang, *Physical Review B* **82**, 045122 (2010).
- ²³ R. Gracia-Abad, S. Sangiao, C. Bigi, S. Kumar Chaluvadi, P. Orgiani, and J. M. De Teresa, *Nanomaterials* **11**, 1077 (2021).
- ²⁴ S. Mao, A. Yamakage, and Y. Kuramoto, *Physical Review B* **84**, 115413 (2011).
- ²⁵ M. Shafiei, F. Fazileh, F. M. Peeters, and M. V. Milošević, *Physical Review Materials* **6**, 074205 (2022).
- ²⁶ M. Shafiei, F. Fazileh, F. M. Peeters, and M. V. Milošević, *Physical Review B* **106**, 035119 (2022).
- ²⁷ Z. Qiao, Y. Han, L. Zhang, K. Wang, X. Deng, H. Jiang, S. A. Yang, J. Wang, and Q. Niu, *Physical Review Letters* **117**, 056802 (2016).
- ²⁸ V. Sacksteder, T. Ohtsuki, and K. Kobayashi, *Physical Review Applied* **3**, 064006 (2015).
- ²⁹ H. Luo, *Advanced topological insulators* (John Wiley & Sons, 2019).
- ³⁰ S. Datta, *Electronic transport in mesoscopic systems* (Cambridge University Press, 1997).
- ³¹ D. A. Ryndyk *et al.*, *Springer Series in Solid-State Sciences* **184** (2016).
- ³² Y. Tokura, K. Yasuda, and A. Tsukazaki, *Nature Reviews Physics* **1**, 126 (2019).
- ³³ R. Noguchi, T. Takahashi, K. Kuroda, M. Ochi, T. Shirasawa, M. Sakano, C. Bareille, M. Nakayama, M. Watson, K. Yaji, *et al.*, *Nature* **566**, 518 (2019).
- ³⁴ Z. Ringel, Y. E. Kraus, and A. Stern, *Physical Review B* **86**, 045102 (2012).
- ³⁵ M. R. Brems, J. Paaske, A. M. Lunde, and M. Willatzen, *New Journal of Physics* **20**, 053041 (2018).
- ³⁶ S. M. Young, S. Chowdhury, E. J. Walter, E. J. Mele, C. L. Kane, and A. M. Rappe, *Physical Review B* **84**, 085106 (2011).
- ³⁷ X. Luo, M. B. Sullivan, and S. Y. Quek, *Physical Review B* **86**, 184111 (2012).
- ³⁸ M. Ohring, *Materials science of thin films* (Elsevier, 2001).
- ³⁹ H. Katsura and T. Koma, *Journal of Mathematical Physics* **57**, 021903 (2016).
- ⁴⁰ B. Sbierski and P. W. Brouwer, *Physical Review B* **89**, 155311 (2014).